Progress In Electromagnetics Research, Vol. 113, 227–249, 2011

ELECTROMAGNETIC TUNNELING IN LOSSLESS TRILAYER STACKS CONTAINING SINGLE-NEGATIVE METAMATERIALS

E. Cojocaru

Department of Theoretical Physics
Horia Hulubei National Institute of Physics and Nuclear Engineering
P. O. Box MG-6, Magurele, Bucharest 077125, Romania

Abstract—We analyze the transverse-electric wave propagation through lossless trilayer stacks containing single-negative (SNG) materials in which only one of the two material constants, permittivity (epsilon) or permeability (mu), is negative. We consider the following combinations: ENG/MNG/ENG, ENG/DPS/MNG, DPS/ENG/DPS, and ENG/DPS/ENG, where ENG refers to epsilon-negative, MNG to mu-negative, and DPS to double-positive media. The transfer matrix formalism is applied. Although the waves are evanescent in the SNG media, combining the SNG layers or the SNG and DPS layers, leads to some unusual features, such as the complete tunneling. Since the symmetrical trilayer is equivalent to a single homogeneous layer, the complete tunneling conditions are easily predicted analytically for the trilayer stacks, and we show that in most of cases, they are rather well applicable to the respective bilayer stacks. The field and the Poynting vector distributions are studied in different trilayers and, in some cases, in the respective bilayers. In particular, we show that the complete tunneling is facilitated theoretically in the electrically thin stacks. Similar results could be obtained for the transverse-magnetic waves and the respective dual combinations by using the duality principle.

1. INTRODUCTION

The electromagnetic wave propagation in metamaterials has recently attracted much attention. The metamaterials include double-negative (DNG) and single-negative (SNG) materials. The DNG materials are artificial composites with both permittivity (ϵ) and permeability (μ)

Received 7 January 2011, Accepted 28 January 2011, Scheduled 2 February 2011
Corresponding author: E. Cojocaru (ecojocaru@theory.nipne.ro).

simultaneously negative, and they were first investigated theoretically by Veselago [1]. The DNG materials exhibit many unusual physical properties which are different from those of conventional double-positive (DPS) right-handed materials [2–6]. In addition to DNG materials, there are also the SNG materials in which only one of the two material parameters ϵ and μ is negative. The SNG materials consist of ϵ-negative (ENG) materials with $\epsilon < 0$ but $\mu > 0$ and μ-negative (MNG) materials with $\mu < 0$ but $\epsilon > 0$. In general, a Drude model is used to describe the isotropic SNG materials,

$$\epsilon = 1 - (\omega_{ep}/\omega)^2 \tag{1}$$

in lossless ENG media, and

$$\mu = 1 - (\omega_{mp}/\omega)^2 \tag{2}$$

in lossless MNG media, where ω is the angular frequency, ω_{ep} and ω_{mp} is the electronic plasma frequency and magnetic plasma frequency, respectively.

The electromagnetic waves are evanescent in the SNG materials, but they are propagating in certain composite structures which are based on the SNG media. Thus, the electromagnetic tunneling has been proved theoretically through the ENG/MNG (or MNG/ENG) bilayers [7–10]. It has been proved also theoretically and experimentally through the ENG/air/MNG (or MNG/air/ENG) trilayers in [11] and through the DPS/ENG/DPS trilayers in [12]. Dispersion properties of ENG/MNG or MNG/ENG multilayers have been analyzed in [13–19].

In this paper, we are concerned with the electromagnetic wave propagation in lossless trilayers which are based on SNG materials. Relations and numerical examples are provided for transverse-electric (TE) polarized propagating waves in the trilayer ENG/MNG/ENG, ENG/DPS/MNG, DPS/ENG/DPS, and ENG/DPS/ENG structures. By applying the duality properties of Maxwell's equations, similar relations could be determined for the transverse-magnetic (TM) polarized waves and the respective dual trilayer MNG/ENG/MNG, MNG/DPS/ENG, DPS/MNG/DPS, and MNG/DPS/MNG structures. In many cases, we compare the behavior of the respective bilayers with that of the symmetrical trilayers.

2. NOTATIONS AND GENERAL RELATIONS

In our analysis the media are assumed lossless, the material constants ϵ and μ being real and relative, dimensionless quantities. Consider a Cartesian coordinate system (x, y, z) with unit vectors $\hat{\mathbf{x}}$, $\hat{\mathbf{y}}$, and $\hat{\mathbf{z}}$, and a monochromatic plane wave with time dependence $\exp(i\omega t)$ in

the free space, with the wave vector $\mathbf{k}_0 = \hat{\mathbf{x}}k_x + \hat{\mathbf{z}}k_{z0}$ in the x-z plane, of magnitude $k_0 = \omega/c$, where c is the velocity of light in vacuum. The x component, $k_x = k_0 \sin\theta_0$, is real and the same for different media of propagation, where θ_0 is the incidence angle; the z component is $k_{z0} = \sqrt{k_0^2 - k_x^2}$. If the medium of propagation is characterized by the material constants (ϵ, μ), the respective z component of the wave vector is

$$\begin{aligned} k_z &\equiv \beta = \sqrt{k_0^2\epsilon\mu - k_x^2} \quad \text{for} \quad k_x^2 < k_0^2\epsilon\mu \\ k_z &\equiv -i\kappa = -i\sqrt{k_x^2 - k_0^2\epsilon\mu} \quad \text{for} \quad k_x^2 > k_0^2\epsilon\mu \end{aligned} \tag{3}$$

As for example, for a plane wave into an SNG medium, either ENG of material constants $(-\epsilon, \mu)$ or MNG of material constants $(\epsilon, -\mu)$, where ϵ and μ are positive numbers, the z component of the wave vector is imaginary, $k_z = -i\kappa$, since for any incidence angle, $k_x^2 > k_0^2\epsilon\mu$.

Consider a stack of J homogeneous and isotropic layers of material constants (ϵ_j, μ_j), where $j = 1, 2, \ldots, J$, lying between the cover and the substrate media, with interfaces parallel to the x-y plane. Since the material variation is only in the z direction, the Maxwell's equations reduce to independent sets of equations for the TE and TM polarizations. As shown in Fig. 1, the TE polarization is distinguished by having the electric-field vector $\mathbf{E}$ perpendicular to the plane of incidence, whereas it is the magnetic-field vector $\mathbf{H}$ that is transverse in the TM case. A set of polarization-dependent parameters ξ_j, U, and V are defined in Table 1 so that the basic relations apply to both polarizations. The tangential field components U and V are continuous

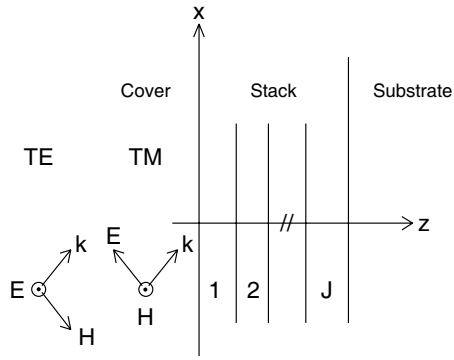

Figure 1. Electric- and magnetic-field vectors for a TE (left) and TM (right) polarized plane wave obliquely incident on a stack of J layers lying between the cover and the substrate media.

Table 1. Polarization-dependent parameters ξ_j, U, and V.

Polarization	ξ_j	U	V
TE	$\frac{k_{zj}}{\eta_0 k_0 \mu_j}$	E_y	$-H_x$
TM	$\frac{\eta_0 k_{zj}}{k_0 \epsilon_j}$	H_y	E_x

across the interfaces and a unimodular field-transfer matrix M_j relates the field amplitudes U_j and V_j at z_j to the corresponding amplitudes at z_{j-1},

$$\begin{bmatrix} U_{j-1} \\ V_{j-1} \end{bmatrix} = M_j \begin{bmatrix} U_j \\ V_j \end{bmatrix} \tag{4}$$

where M_j is given by [20],

$$M_j = \begin{bmatrix} \cos\phi_j & (i/\xi_j)\sin\phi_j \\ i\xi_j \sin\phi_j & \cos\phi_j \end{bmatrix} \tag{5}$$

with $\phi_j = k_{zj}(z_j - z_{j-1})$, k_{zj} denoting the respective z component of the wave vector,

$$\xi_j = \begin{cases} k_{zj}/(\eta_0 k_0 \mu_j) & \text{for } TE \\ \eta_0 k_{zj}/(k_0 \epsilon_j) & \text{for } TM \end{cases} \tag{6}$$

where $\eta_0 = \sqrt{\mu_0/\epsilon_0}$ is the intrinsic impedance of the free space. When the jth layer is an SNG medium, either ENG or MNG, since k_{zj} is imaginary, ξ_j and ϕ_j are also imaginary. Thus, for an SNG layer, we use notation

$$\phi_j = -i\varphi_j \tag{7}$$

and the following relations

$$\begin{aligned} &\cos(-i\varphi_j) = \cosh\varphi_j, \qquad \sin(-i\varphi_j) = -i\sinh\varphi_j, \\ &\tan(-i\varphi_j) = -i\tanh\varphi_j. \end{aligned} \tag{8}$$

The transfer matrix of the stack consisting of J layers is given by the product of the respective transfer matrices for the individual layers,

$$M = \prod_{j=1}^{J} M_j \tag{9}$$

If we denote by m_{ij}, with $i,\ j = 1, 2$, the elements of the matrix M, expressions for the amplitude reflection and transmission coefficients (r_{cs} and t_{cs}) are readily derived up to a phase factor,

$$r_{cs} = \frac{\xi_c m_{11} + \xi_c \xi_s m_{12} - m_{21} - \xi_s m_{22}}{\xi_c m_{11} + \xi_c \xi_s m_{12} + m_{21} + \xi_s m_{22}} \tag{10}$$

$$t_{cs} = \frac{2\xi_c}{\xi_c m_{11} + \xi_c \xi_s m_{12} + m_{21} + \xi_s m_{22}} \tag{11}$$

where the subscripts c and s refer to the cover and the substrate, respectively. The reflectance R and the transmittance T are given by

$$R = |r_{cs}|^2, \qquad T = \frac{\text{Real}(\xi_s)}{\text{Real}(\xi_c)} |t_{cs}|^2 \tag{12}$$

Detailed expressions for the tangential components of the electric and magnetic fields into a trilayer stack for the TE polarization are given in Appendix A. For simplicity, in the following we consider the trilayers are embedded in air, that is, $\xi_c = \xi_s = \xi_0$. For a trilayer stack, the matrix elements m_{11} and m_{22} are given by relation

$$\begin{aligned}\begin{pmatrix} m_{11} \\ m_{22} \end{pmatrix} &= \cos\phi_1 \cos\phi_2 \cos\phi_3 - \begin{pmatrix} \xi_3/\xi_2 \\ \xi_2/\xi_3 \end{pmatrix} \cos\phi_1 \sin\phi_2 \sin\phi_3 \\ &\quad - \begin{pmatrix} \xi_3/\xi_1 \\ \xi_1/\xi_3 \end{pmatrix} \cos\phi_2 \sin\phi_1 \sin\phi_3 - \begin{pmatrix} \xi_2/\xi_1 \\ \xi_1/\xi_2 \end{pmatrix} \cos\phi_3 \sin\phi_1 \sin\phi_2 \end{aligned} \tag{13}$$

and the matrix elements m_{12} and m_{21} by relation

$$\begin{aligned}\begin{pmatrix} m_{12} \\ m_{21} \end{pmatrix} &= i \Bigg[\begin{pmatrix} 1/\xi_1 \\ \xi_1 \end{pmatrix} \cos\phi_2 \cos\phi_3 \sin\phi_1 + \begin{pmatrix} 1/\xi_2 \\ \xi_2 \end{pmatrix} \cos\phi_1 \cos\phi_3 \sin\phi_2 \\ &\quad + \begin{pmatrix} 1/\xi_3 \\ \xi_3 \end{pmatrix} \cos\phi_1 \cos\phi_2 \sin\phi_3 - \begin{pmatrix} \xi_2/(\xi_1\xi_3) \\ \xi_1\xi_3/\xi_2 \end{pmatrix} \sin\phi_1 \sin\phi_2 \sin\phi_3 \Bigg] \end{aligned} \tag{14}$$

When all layers are electrically thin, $|\phi_j| \leq 0.1$, with $j = 1, 2, 3$, the matrix M of the trilayer becomes

$$M \approx \begin{bmatrix} 1 & i\sum_{j=1}^{3} \phi_j/\xi_j \\ i\sum_{j=1}^{3} \phi_j \xi_j & 1 \end{bmatrix} \tag{15}$$

and the trilayer is equivalent to a single layer of thickness d_{eq} and material constants $(\epsilon_{eq}, \mu_{eq})$ determined by

$$\begin{aligned} \mu_{eq} &= \sum_{j=1}^{3} p_j \mu_j, \\ \epsilon_{eq} &= \sum_{j=1}^{3} p_j \epsilon_j - \frac{k_x^2}{k_0^2} \left[\sum_{j=1}^{3} \frac{p_j}{\mu_j} - \frac{1}{\sum_{j=1}^{3} p_j \mu_j} \right] \end{aligned} \tag{16}$$

where $p_j = d_j/d_{eq}$, d_j being the thickness of the jth layer. For an electrically thin bilayer [21], one can use (16) with two terms in the

sums. The complete tunneling through the electrically thin trilayer, with the transfer matrix approximated by (15), is achieved either when

$$m_{12} = m_{21} = 0 \tag{17}$$

in which case the trilayer stack behaves like an absentee layer, or when

$$m_{12}\xi_0^2 - m_{21} = 0 \tag{18}$$

For TE polarization, relation (15) becomes at normal incidence

$$M \approx \begin{bmatrix} 1 & i\eta_0 k_0 \sum_{j=1}^{3} d_j \mu_j \\ i(k_0/\eta_0) \sum_{j=1}^{3} d_j \epsilon_j & 1 \end{bmatrix} \tag{19}$$

Applying (17) gives the following approximate conditions for the complete tunneling through an electrically thin trilayer

$$\sum_{j=1}^{3} d_j \mu_j = 0, \qquad \sum_{j=1}^{3} d_j \epsilon_j = 0 \tag{20}$$

3. TUNNELING THROUGH THE TRILAYER ENG/MNG/ENG STRUCTURE

Consider a symmetrical trilayer of material constants $(-\epsilon_1, \mu_1)/(\epsilon_2, -\mu_2)/(-\epsilon_1, \mu_1)$ and layers thicknesses $d_1/d_2/d_1$, where ϵ_j and μ_j, with $j = 1, 2$, are positive numbers. Then,

$$\begin{aligned} &\xi_1 = \xi_3 = -i\kappa_1/(\eta_0\mu_1), \qquad \xi_2 = i\kappa_2/(\eta_0\mu_2), \\ &\phi_j = -i\kappa_j d_j = -i\varphi_j, \quad j = 1, 2. \end{aligned} \tag{21}$$

From (13) and (14), one obtains at normal incidence

$$\begin{aligned} m_{11} =& m_{22} = \cosh 2\varphi_1 \cosh \varphi_2 - \frac{1}{2}\left(\frac{\eta_1}{\eta_2} + \frac{\eta_2}{\eta_1}\right) \sinh 2\varphi_1 \sinh \varphi_2 \\ \begin{pmatrix} m_{12} \\ m_{21} \end{pmatrix} =& \frac{i}{2\eta_2} \begin{pmatrix} \eta_0 \\ -1/\left(\eta_0 \eta_1^2\right) \end{pmatrix} \Bigg[2\eta_1\eta_2 \cosh \varphi_2 \sinh 2\varphi_1 \\ &+ \begin{pmatrix} 1 \\ -1 \end{pmatrix} \left(\eta_1^2 - \eta_2^2\right) \sinh \varphi_2 - \left(\eta_1^2 + \eta_2^2\right) \cosh 2\varphi_1 \sinh \varphi_2 \Bigg] \\ \eta_j =& \sqrt{\mu_j/\epsilon_j}, \qquad j = 1, 2 \end{aligned} \tag{22}$$

The condition (18) for complete tunneling will be satisfied when

$$\varphi_2 = 2\varphi_1 \quad \text{and} \quad \eta_1 = \eta_2 \tag{23}$$

which is similar to the "matched pair" condition established in [7] for the ENG/MNG bilayer. From (22), we obtain a further condition

for the complete tunneling through the symmetrical ENG/MNG/ENG trilayer,

$$\tanh\varphi_2 = \frac{\frac{2\eta_1\eta_2}{\eta_1^2+\eta_2^2}\sinh 2\varphi_1}{\frac{1-\eta_1^2}{1+\eta_1^2}\frac{\eta_1^2-\eta_2^2}{\eta_1^2+\eta_2^2}+\cosh 2\varphi_1} \tag{24}$$

The matched trilayer condition (23) results as a specific case from the more general condition (24). From the matched trilayer condition (23) one obtains

$$\frac{2d_1}{d_2} = \frac{\mu_2}{\mu_1} = \frac{\epsilon_2}{\epsilon_1} \tag{25}$$

The following conditions result for a conjugate matched trilayer [7]

$$2d_1 = d_2, \qquad \mu_2 = \mu_1, \qquad \epsilon_2 = \epsilon_1. \tag{26}$$

Thus, for the conjugate matched ENG/MNG/ENG trilayer of material constants $(-\epsilon,\mu)/(\epsilon,-\mu)/(-\epsilon,\mu)$, where ϵ and μ are positive numbers, and layers thicknesses $\frac{d}{2}/d/\frac{d}{2}$, the complete tunneling will occur at any incidence angle [7]. Relation (25) can be written in a general form

$$\frac{p2d_1}{qd_2} = \frac{p\mu_2}{q\mu_1} = \frac{p\epsilon_2}{q\epsilon_1} \tag{27}$$

which means that, if a trilayer of material constants $(-\epsilon_1,\mu_1)/(\epsilon_2,-\mu_2)/(-\epsilon_1,\mu_1)$ and layers thicknesses $d_1/d_2/d_1$ allows the complete tunneling at normal incidence, then the trilayer of material constants $(-q\epsilon_1,q\mu_1)/(p\epsilon_2,-p\mu_2)/(-q\epsilon_1,q\mu_1)$ and layers thicknesses $\frac{d_1}{q}/\frac{d_2}{p}/\frac{d_1}{q}$, with p and q integer numbers, will allow the complete tunneling at normal incidence also. Numerical examples are given in Fig. 2(a). Curve 1 corresponds to a conjugate matched trilayer. One can see that the complete tunneling occurs at any incidence angle. Curve 2 corresponds to a matched trilayer of parameters determined from those of the conjugate matched trilayer, represented by curve 1, by applying relation (27) with $p = 2$ and $q = 4$. The complete tunneling is achieved on a large interval of θ_0 variation. Curve 3 corresponds to another matched trilayer of parameters determined also from those of the conjugate matched trilayer by applying relation (27) with $p = 1/4$ and $q = 1/2$. The complete tunneling is achieved on a narrower interval of θ_0 variation. The inset in Fig. 2(a) illustrates the evanescent wave into an MNG layer. By comparison, Fig. 2(b) shows the complete tunneling through the respective bilayers. A larger interval of θ_0 variation is allowed for the matched trilayers in comparison with the respective matched bilayers.

Figure 3 shows comparatively the electric field, the magnetic field, and the z component of the Poynting vector for a normally incident

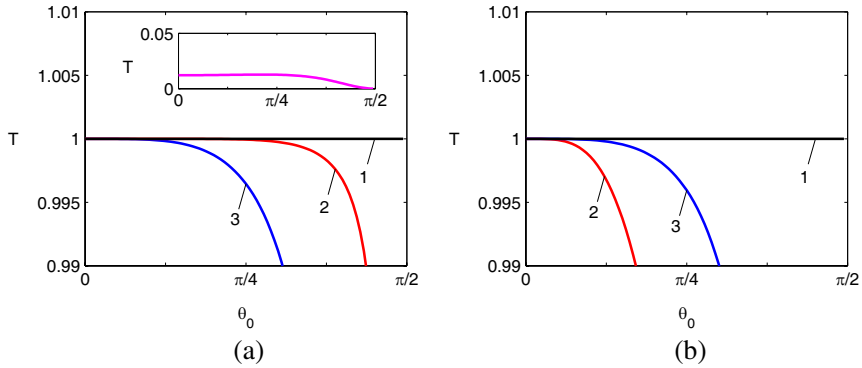

Figure 2. (a) The transmittance T against the incidence angle θ_0 at $\omega = 5\,\mathrm{GHz}$ for different ENG/MNG/ENG trilayers of given material constants and layers thicknesses in mm: 1 — $(-3, 6)/(3, -6)/(-3, 6)$ and 20/40/20 thick; 2 — $(-12, 24)/(6, -12)/(-12, 24)$ and 5/20/5 thick; 3 — $(-1.5, 3)/(0.75, -1.5)/(-1.5, 3)$ and 5/20/5 thick. The inset shows T against θ_0 for a single MNG layer of material constants $(3, -6)$ and 40 mm thick. (b) The same like in (a) but for the respective ENG/MNG bilayers of layers thicknesses in mm: 1 — 40/40; 2 and 3 — 10/20.

plane wave onto the conjugate matched ENG/MNG/ENG trilayer and the respective conjugate matched ENG/MNG bilayer. In both cases, the field is predominantly concentrated around the interfaces between the SNG layers. The real part of the Poynting vector is uniform and equal unity through the structures, indicating the complete tunneling. The imaginary part of the Poynting vector is zero in the free space, it is only present inside the slabs and has its peaks at the interfaces between the SNG layers [7]. The fields and the imaginary part of the Poynting vector take smaller values inside the conjugate matched trilayer than inside the respective conjugate matched bilayer.

Figure 4 shows the complete tunneling through different electrically thin ENG/MNG/ENG trilayers and the respective ENG/MNG bilayers. The parameters of trilayers are determined from those of the conjugate matched trilayer, represented by curve 1 in Fig. 4(a), by applying relations (27) and (20). One can see that in both cases of electrically thin trilayers and bilayers, the complete tunneling is attained on large intervals of θ_0 variation.

Figure 5 shows the electric field, the magnetic field, and the S_z component at normal incidence for the conjugate matched electrically thin trilayer and an asymmetrical trilayer. The field is predominantly concentrated around the interfaces between the SNG layers, the

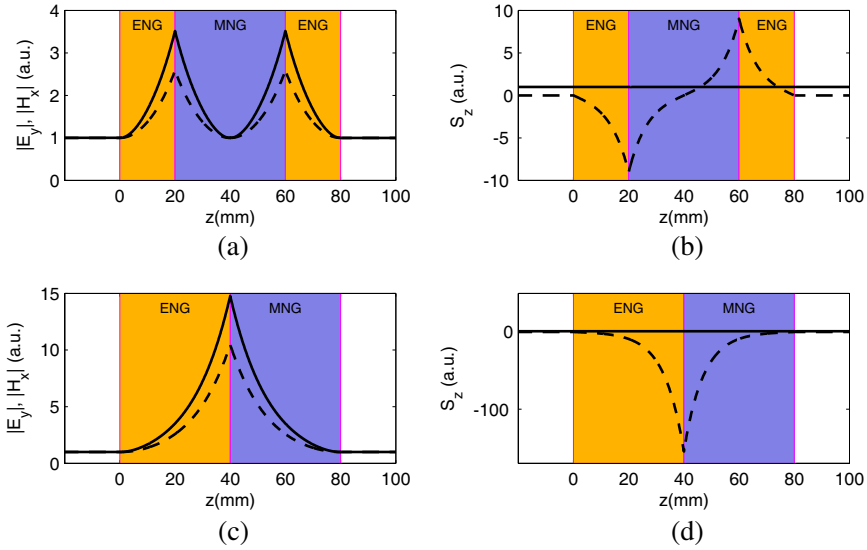

Figure 3. (a) The electric field $|E_y|$ (solid curve) and the magnetic field $|H_x|$ (dashed curve); (b) the real (solid curve) and the imaginary (dashed curve) z component S_z of the Poynting vector into the conjugate matched ENG/MNG/ENG trilayer represented by curve 1 in Fig. 2(a). Similarly in (c) and (d), but for the conjugate matched ENG/MNG bilayer represented by curve 1 in Fig. 2(b).

magnetic field attaining greater values in comparison with the electric field. For the asymmetrical trilayer, the field is greater at the interface of the MNG layer with the thicker ENG layer. The fields and the imaginary part of S_z take smaller values inside the electrically thin trilayers than inside the electrically thick trilayers [see Figs. 3(a) and (b)].

4. TUNNELING THROUGH THE TRILAYER ENG/DPS/MNG STRUCTURE.

Consider the trilayer of material constants $(-\epsilon_1, \mu_1)/(\epsilon_2, \mu_2)/(\epsilon_3, -\mu_3)$ and layers thicknesses $d_1/d_2/d_3$, where ϵ_j and μ_j, with $j = 1, 2, 3$, are positive numbers. From (13) and (14), one obtains at normal incidence

$$\begin{pmatrix} m_{11} \\ m_{22} \end{pmatrix} = \cos\phi_2 \cosh\varphi_1 \cosh\varphi_3 - \begin{pmatrix} \eta_2/\eta_3 \\ -\eta_3/\eta_2 \end{pmatrix} \sin\phi_2 \cosh\varphi_1 \sinh\varphi_3$$
$$-\begin{pmatrix} \eta_1/\eta_3 \\ \eta_3/\eta_1 \end{pmatrix} \cos\phi_2 \sinh\varphi_1 \sinh\varphi_3 - \begin{pmatrix} \eta_1/\eta_2 \\ -\eta_2/\eta_1 \end{pmatrix} \sin\phi_2 \cosh\varphi_3 \sinh\varphi_1 \quad (28)$$

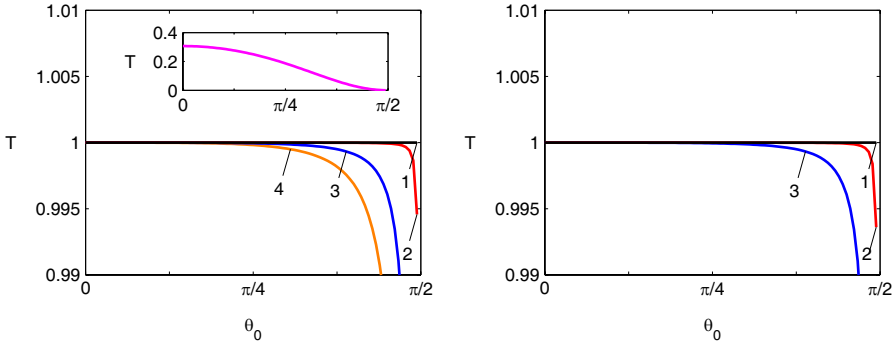

Figure 4. (a) The transmittance T against θ_0 at $\omega = 0.3\,\mathrm{GHz}$ for the ENG/MNG/ENG trilayers of given material constants and layers thicknesses in mm: 1 — $(-68, 3)/(68, -3)/(-68, 3)$ and 20/40/20 thick; 2 — $(-272, 12)/(136, -6)/(-272, 12)$ and 5/20/5 thick; 3 — $(-34, 1.5)/(17, -0.75)/(-34, 1.5)$ and 5/20/5 thick; 4 — $(-68, 3)/(28, -1.1667)/(-50, 2)$ and 10/60/20 thick. The inset shows T against θ_0 for a single MNG layer of material constants $(68, -3)$ and 40 mm thick. (b) The same like 1, 2, and 3 in (a), but for the respective ENG/MNG bilayers of layers thicknesses in mm: 1 — 40/40; 2 and 3 — 10/20.

$$\begin{pmatrix} m_{12} \\ m_{21} \end{pmatrix} = i \begin{pmatrix} \eta_0 \\ 1/\eta_0 \end{pmatrix} \left[\begin{pmatrix} \eta_1 \\ -1/\eta_1 \end{pmatrix} \cos\phi_2 \cosh\varphi_3 \sinh\varphi_1 \right.$$
$$+ \begin{pmatrix} \eta_2 \\ 1/\eta_2 \end{pmatrix} \sin\phi_2 \cosh\varphi_1 \cosh\varphi_3 - \begin{pmatrix} \eta_3 \\ -1/\eta_3 \end{pmatrix} \cos\phi_2 \cosh\varphi_1 \sinh\varphi_3$$
$$\left. + \begin{pmatrix} \eta_1\eta_3/\eta_2 \\ \eta_2/(\eta_1\eta_3) \end{pmatrix} \sin\phi_2 \sinh\varphi_1 \sinh\varphi_3 \right] \tag{29}$$

The complete tunneling is achieved when

$$\eta_2 = 1, \quad \varphi_1 = \varphi_3, \quad \text{and} \quad \eta_3 = 1/\eta_1 \tag{30}$$

where η_j, with $j = 1, 2, 3$, is defined in (22). Furthermore, the parameters φ_1, ϕ_2, and η_1 must satisfy relation

$$\tan\phi_2 = \frac{1}{2}\left(\frac{1}{\eta_1} - \eta_1\right) \tanh\varphi_1 \tag{31}$$

From (30) and (31), one can infer that the complete tunneling at normal incidence is achieved with an ENG/DPS/MNG trilayer of material constants $(-\epsilon_1, \mu_1)/(1, 1)/(\mu_1, -\epsilon_1)$ and layers thicknesses

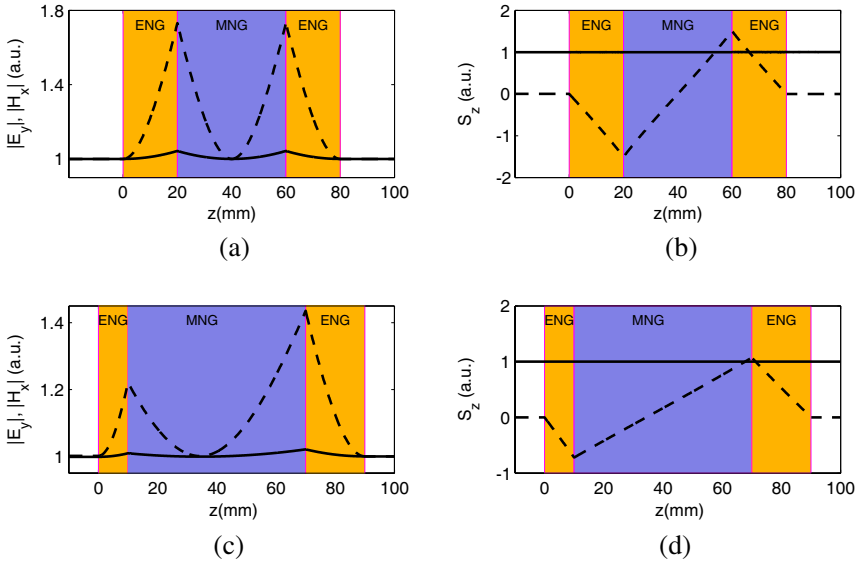

Figure 5. (a) The electric field $|E_y|$ (solid curve) and the magnetic field $|H_x|$ (dashed curve); (b) the real (solid curve) and the imaginary (dashed curve) z component S_z of the Poynting vector into the ENG/MNG/ENG trilayer represented by curve 1 in Fig. 4(a). Similarly in (c) and (d), but for the asymmetrical trilayer represented by curve 4 in Fig. 4(a).

$d_1/d_2/d_1$, where η_1, d_1, and d_2 satisfy relation (31). Note that the air DPS layer of $\eta_2 = 1$ could be a metamaterial of equal positive material constants, $\epsilon_2 = \mu_2$.

Numerical examples are shown in Fig. 6. By keeping d_2 constant, the smaller is d_1, the lower and the broader is the complete tunneling frequency [see Figs. 6(a) and (c)]. When the DPS layer is a dielectric material with $\mu_2 = 1$, by keeping d_1 and d_2 constant, the greater is ϵ_2, the lower is the tunneling frequency and the more incomplete is the tunneling [see Figs. 6(b) and (d)]. Note that all dependencies in Fig. 6 and in the following figures refer to the lowest order frequencies. The dependence of the transmittance on the incidence angle θ_0 is shown in Fig. 7 at different thicknesses of the DPS layer. The greater is the thickness d_2, the narrower is the interval of θ_0 variation for a complete tunneling. At the same thickness d_2 of the DPS layer, the SNG layers are about two times electrically thicker at $\omega_{ep} = \omega_{mp} = 20\,\text{GHz}$ than at $\omega_{ep} = \omega_{mp} = 10\,\text{GHz}$, leading to a narrowing of the interval of θ_0 variation for a complete tunneling in Fig. 7(b) in comparison with Fig. 7(a).

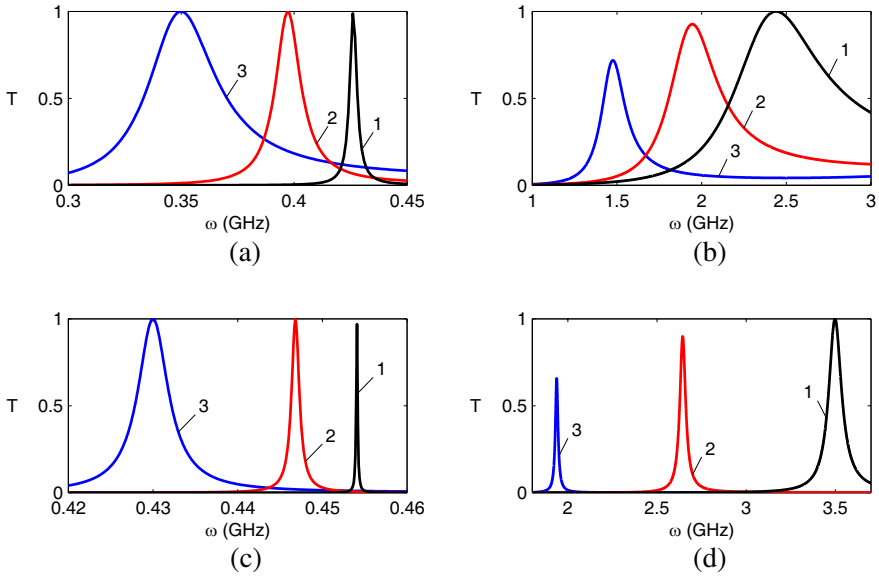

Figure 6. (a) The transmittance T against ω for ENG/DPS/MNG trilayers with an air DPS layer 1000 mm thick and the two SNG layers of material constants determined by (1) and (2) with $\omega_{ep} = \omega_{mp} = 10$ GHz, $\mu_1 = \epsilon_3 = 1$, and of equal $d_1 = d_3$ but varied thickness in mm: 1 — $d_1 = 20$; 2 — $d_1 = 10$; 3 — $d_1 = 5$. (b) The same like in (a), but with both SNG layers 20 mm thick and the DPS layer 100 mm thick of $\mu_2 = 1$ and varied ϵ_2: 1 — $\epsilon_2 = 1$; 2 — $\epsilon_2 = 2$; 3 — $\epsilon_2 = 4$. (c) and (d) the same like in (a) and (b), but when $\omega_{ep} = \omega_{mp} = 20$ GHz.

Figure 8 shows the electric field, the magnetic field, and the z component of the Poynting vector for a normally incident plane wave onto the ENG/DPS/MNG trilayer with an air DPS layer and layers thicknesses $d_1 = d_2 = d_3$, at two circular frequencies. As it was shown in [11], the magnetic field is maximum at the ENG/DPS interface, whereas the electric field has the same maximum value, but at the DPS/MNG interface. The real part of the Poynting vector is uniform and equal unity through the structures. The imaginary part of the Poynting vector is zero in the free space and has a broad peak, being almost constant, inside the DPS layer.

Figure 9 shows the tunneling through different electrically thin ENG/DPS/MNG trilayers of parameters determined by relations (30), (31), and (20). Although the tunneling at normal incidence is not complete in some cases, a rather good tunneling ($T > 0.98$) is achieved on a large interval of θ_0 variation.

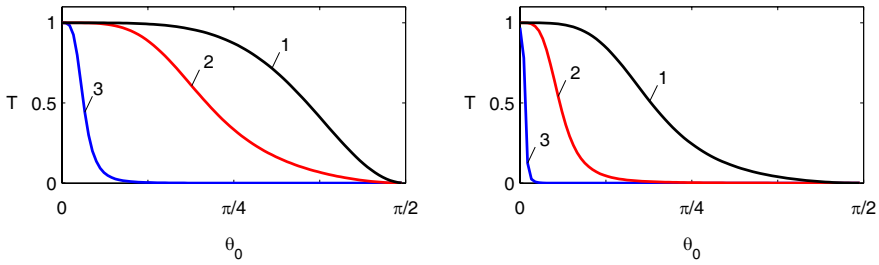

Figure 7. (a) The transmittance T against θ_0 for ENG/DPS/MNG trilayers with the two SNG layers 20 mm thick of material constants $(-\epsilon_1, 1)$ and $(1, -\epsilon_1)$ determined by (1) and (2) with $\omega_{ep} = \omega_{mp} = 10$ GHz, at frequency ω in GHz determined by (31), and the air DPS layer of varied thickness d_2 in mm: 1 — $d_2 = 20$, $\omega \approx 4.82$, $\epsilon_1 \approx 3.3$; 2 — $d_2 = 100$, $\omega \approx 2.44$, $\epsilon_1 \approx 15.8$; 3 — $d_2 = 1000$, $\omega \approx 0.42$, $\epsilon_1 \approx 549.5$. (b) The same like in (a), but when $\omega_{ep} = \omega_{mp} = 20$ GHz: 1 — $d_2 = 20$, $\omega \approx 8.72$, $\epsilon_1 \approx 4.2$; 2 — $d_2 = 100$, $\omega \approx 3.5$, $\epsilon_1 \approx 31.7$; 3 — $d_2 = 1000$, $\omega \approx 0.45$, $\epsilon_1 \approx 1938.8$.

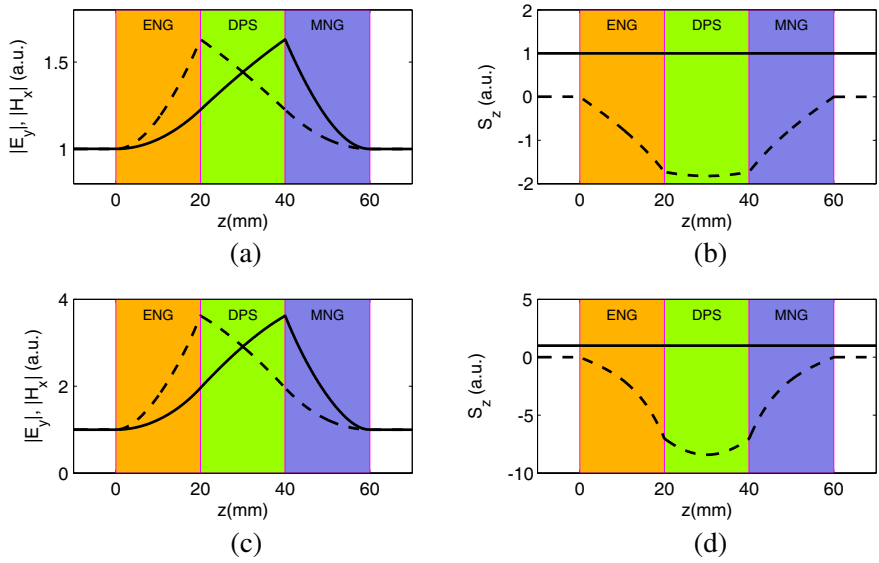

Figure 8. (a) The electric field $|E_y|$ (solid curve) and the magnetic field $|H_x|$ (dashed curve); (b) the real (solid curve) and the imaginary (dashed curve) z component S_z of the Poynting vector into the ENG/DPS/MNG trilayer represented by curve 1 in Fig. 7(a). Similarly in (c) and (d), but for the structure represented by curve 1 in Fig. 7(b).

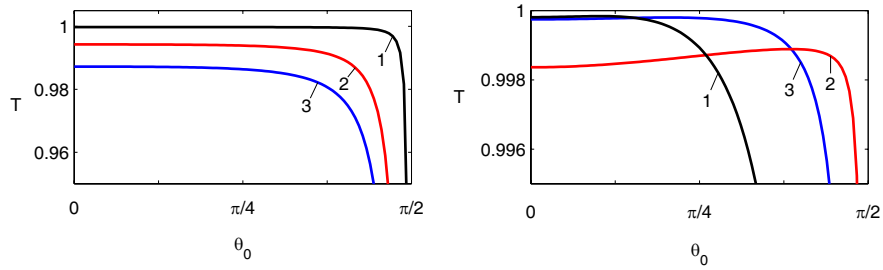

Figure 9. (a) The transmittance T against θ_0 at $\omega = 0.3\,\mathrm{GHz}$ for the ENG/DPS/MNG trilayer of material constants $(-68, 3)/(1, 1)/(68, -3)$ with the two SNG layers 10 mm thick and the air DPS layer of varied d_2 thickness in mm: 1 — $d_2 = 10$; 2 — $d_2 = 100$; 3 — $d_2 = 150$. (b) T against θ_0 at $\omega = 0.3\,\mathrm{GHz}$ for different ENG/DPS/MNG trilayers of given material constants and layers thicknesses in mm: 1 — $(-68, 3)/(1, 1)/(63, -8)$ and 20/40/20 thick; 2 — $(-68, 3)/(1, 1)/(66, -5)$ and 20/40/20 thick; 3 — $(-68, 3)/(1, 1)/(32, -3.5)$ and 10/40/20 thick.

5. TUNNELING THROUGH THE TRILAYER DPS/ENG/DPS STRUCTURE

Consider a symmetrical trilayer of material constants $(\epsilon_1, \mu_1)/(-\epsilon_2, \mu_2)/(\epsilon_1, \mu_1)$ and layers thicknesses $d_1/d_2/d_1$, where ϵ_j and μ_j, with $j = 1, 2$, are positive numbers. From (13) and (14), one obtains at normal incidence

$$\begin{aligned} m_{11} =& m_{22} = \cos 2\phi_1 \cosh\varphi_2 + \frac{1}{2}\left(\frac{\eta_1}{\eta_2} - \frac{\eta_2}{\eta_1}\right)\sin 2\phi_1 \sinh\varphi_2 \\ \begin{pmatrix} m_{12} \\ m_{21} \end{pmatrix} =& \frac{i}{2\eta_2}\begin{pmatrix} \eta_0 \\ 1/(\eta_0\eta_1^2) \end{pmatrix}\Bigg[2\eta_1\eta_2 \sin 2\phi_1 \cosh\varphi_2 \\ &+ \begin{pmatrix} 1 \\ -1 \end{pmatrix}(\eta_1^2 + \eta_2^2)\sinh\varphi_2 - (\eta_1^2 - \eta_2^2)\cos 2\phi_1 \sinh\varphi_2\Bigg] \end{aligned} \tag{32}$$

where η_j, with $j = 1, 2$, is defined in (22). Applying condition (18) for complete tunneling gives

$$\tanh\varphi_2 = \frac{\frac{2\eta_1\eta_2}{\eta_1^2+\eta_2^2}\sin 2\phi_1}{\frac{1+\eta_1^2}{1-\eta_1^2} + \frac{\eta_1^2-\eta_2^2}{\eta_1^2+\eta_2^2}\cos 2\phi_1} \tag{33}$$

Numerical examples are shown in Fig. 10(a) for a symmetrical

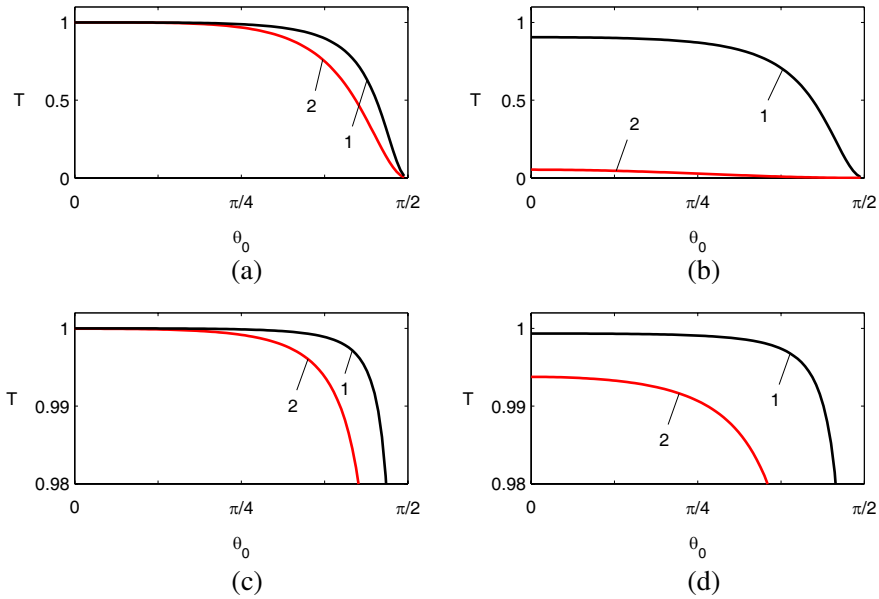

Figure 10. (a) The transmittance T against θ_0 at $\omega = 5\,\mathrm{GHz}$ for symmetrical DPS/ENG/DPS trilayers of material constants: 1 — $(8.2, 1)/(-5, 2)/(8.2, 1)$; 2 — $(59.57, 1)/(-5, 2)/(59.57, 1)$; and layers thicknesses 5/10/5 in mm. (b) The same like in (a), but for the respective DPS/ENG bilayers of layers thicknesses 10/10 in mm. (c) T against θ_0 at $\omega = 0.3\,\mathrm{GHz}$ for symmetrical DPS/ENG/DPS trilayers of given material constants and layers thicknesses in mm: 1 — $(36.5, 1)/(-68, 3)/(36.5, 1)$ and 20/20/20 thick; 2 — $(18.75, 1)/(-68, 3)/(18.75, 1)$ and 20/10/20 thick. (d) The same like in (c), but for the respective DPS/ENG bilayers of layers thicknesses in mm: 1 — 40/20; 2 — 40/10.

DPS/ENG/DPS trilayer with dielectric DPS layers ($\mu_1 = 1$) and an ENG layer of given material constants $(-\epsilon_2, \mu_2)$. As it was shown in [12], two values of ϵ_1 satisfying (33) at given d_1 and d_2 could exist. Curves 1 and 2 in Fig. 10(a) correspond to these values of ϵ_1, curve 1 corresponding to the smaller value of ϵ_1. The complete tunneling is achieved on a larger interval of θ_0 variation for the smaller value of ϵ_1. By comparison, Fig. 10(b) shows the tunneling through the respective DPS/ENG bilayers. For the smaller value of ϵ_1 there is a tunneling through the bilayer, but for the greater value of ϵ_1 the wave is evanescent. Results are shown in Figs. 10(c) and (d) for electrically thin structures. The complete tunneling is achieved on a larger interval of θ_0 variation for both values of ϵ_1 in case of electrically thin trilayers in

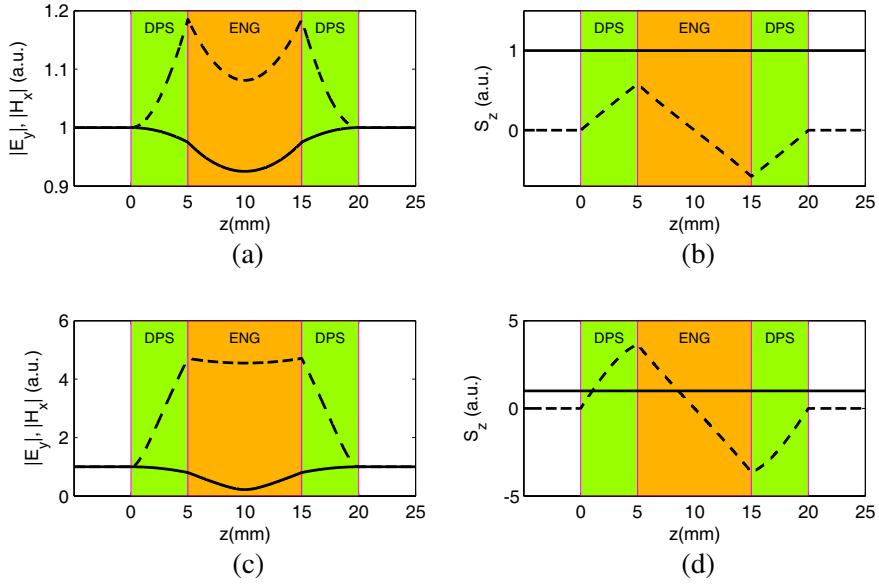

Figure 11. (a) The electric field $|E_y|$ (solid curve) and the magnetic field $|H_x|$ (dashed curve); (b) the real (solid curve) and the imaginary (dashed curve) z component S_z of the Poynting vector into the DPS/ENG/DPS trilayer represented by curve 1 in Fig. 10(a). Similarly in (c) and (d), but for the trilayer represented by curve 2 in Fig. 10(a).

comparison with the electrically thick trilayers of Fig. 10(a). An almost complete tunneling ($T > 0.99$) occurs in the respective electrically thin bilayers for both values of ϵ_1.

Figure 11 shows the electric field, the magnetic field, and the z component of the Poynting vector for a normally incident plane wave onto the DPS/ENG/DPS trilayers represented by curves 1 and 2 in Fig. 10(a). The electric field has a broad minimum inside the ENG layer, whereas the magnetic field is much larger, with peaks at the two DPS/ENG interfaces. The real part of the Poynting vector is uniform and equal unity through the structure, indicating the complete tunneling. The imaginary part of the Poynting vector has its peaks at the DPS/ENG interfaces.

6. TUNNELING THROUGH THE TRILAYER ENG/DPS/ENG STRUCTURE

Consider a symmetrical trilayer of the material constants $(-\epsilon_1, \mu_1)$ $/(\epsilon_2, \mu_2)/(-\epsilon_1, \mu_1)$ and layers thicknesses $d_1/d_2/d_1$, where ϵ_j and μ_j,

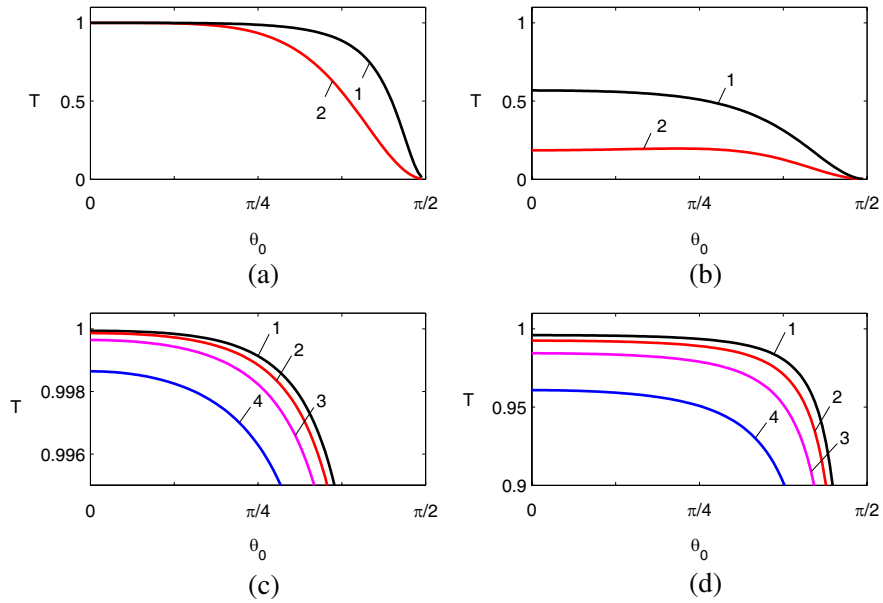

Figure 12. (a) The transmittance T against θ_0 at $\omega = 5\,\mathrm{GHz}$ for symmetrical ENG/DPS/ENG trilayers of layers thicknesses 10/5/10 in mm and material constants: 1 — $(-5, 2)/(23.6, 1)/(-5, 2)$; 2 — $(-3, 6)/(17.7, 1)/(-3, 6)$. (b) The same like in (a), but for the respective ENG/DPS bilayers of layers thicknesses 20/5 in mm. (c) T against θ_0 at $\omega = 0.3\,\mathrm{GHz}$ for symmetrical ENG/DPS/ENG trilayers of material constants $(-68, 3)/(\epsilon_2, 1)/(-68, 3)$ and layers thicknesses $10/d_2/10$ in mm with varied d_2 and ϵ_2 determined from (35): 1 — $d_2 = 20$, $\epsilon_2 = 72$; 2 — $d_2 = 50$, $\epsilon_2 = 29.4$; 3 — $d_2 = 100$, $\epsilon_2 = 15.2$; 4 — $d_2 = 200$, $\epsilon_2 = 8.1$. (d) The same like in (c), but for the respective ENG/DPS bilayers of layers thicknesses $20/d_2$ in mm.

with $j = 1, 2$, are positive numbers. From (13) and (14), one obtains at normal incidence

$$\begin{aligned} m_{11} =& m_{22} = \cos\phi_2 \cosh 2\varphi_1 - \frac{1}{2}\left(\frac{\eta_1}{\eta_2} - \frac{\eta_2}{\eta_1}\right)\sin\phi_2 \sinh 2\varphi_1 \\ \begin{pmatrix} m_{12} \\ m_{21} \end{pmatrix} =& \frac{i}{2\eta_2}\begin{pmatrix} \eta_0 \\ -1/(\eta_0\eta_1^2) \end{pmatrix}\left[2\eta_1\eta_2 \cos\phi_2 \sinh 2\varphi_1\right. \\ &\left. + \begin{pmatrix} 1 \\ -1 \end{pmatrix}\left(\eta_1^2 + \eta_2^2\right)\sin\phi_2 - \left(\eta_1^2 - \eta_2^2\right)\sin\phi_2 \cosh 2\varphi_1\right] \end{aligned} \tag{34}$$

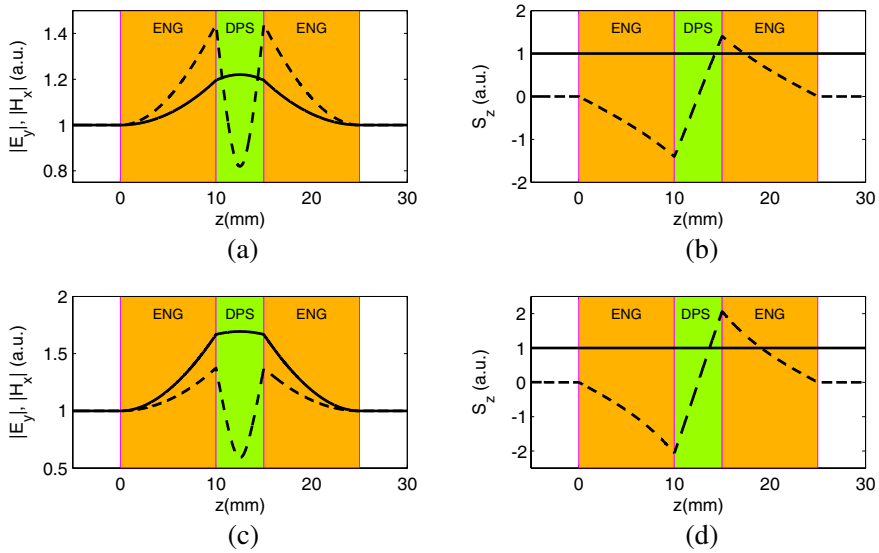

Figure 13. (a) The electric field $|E_y|$ (solid curve) and the magnetic field $|H_x|$ (dashed curve); (b) the real (solid curve) and the imaginary (dashed curve) z component S_z of the Poynting vector into the ENG/DPS/ENG trilayer represented by curve 1 in Fig. 12(a). Similarly in (c) and (d), but for the trilayer represented by curve 2 in Fig. 12(a).

where η_j, with $j = 1, 2$, is defined in (22). Applying condition (18) for complete tunneling gives a relation similar to (33)

$$\tan\phi_2 = \frac{\frac{2\eta_1\eta_2}{\eta_1^2+\eta_2^2}\sinh 2\varphi_1}{\frac{1-\eta_1^2}{1+\eta_1^2} + \frac{\eta_1^2-\eta_2^2}{\eta_1^2+\eta_2^2}\cosh 2\varphi_1} \tag{35}$$

Numerical examples are shown in Fig. 12(a) for two symmetrical ENG/DPS/ENG trilayers with a dielectric DPS layer of ($\mu_2 = 1$) and ϵ_2 determined by (35) at given $-\epsilon_1$, μ_1, d_1, and d_2. By comparison, Fig. 12(b) shows the transmittance of the respective ENG/DPS bilayers. The tunneling is clearly better through the symmetrical trilayers than through the respective bilayers. Figs. 12(c) and (d) shows the behavior of T against θ_0 for electrically thin trilayers and the respective bilayers. At given $-\epsilon_1$, μ_1, and d_1, the thickness d_2 of the dielectric DPS layer is varied and the respective value of ϵ_2 is determined from (35). The thinner is the DPS layer, the better is the tunneling through the trilayers and the respective bilayers.

Figure 13 shows the electric field, the magnetic field, and the z component of the Poynting vector for a normally incident plane wave onto the ENG/DPS/ENG trilayers represented by curves 1 and 2 in Fig. 12(a). The electric field is maximum whereas the magnetic field is minimum at the middle of the DPS layer. The electric field has a smooth variation, whereas the magnetic field has a strong variation, with peaks at the two ENG/DPS interfaces, and the minimum at the middle of the DPS layer. The real part of the Poynting vector is uniform and equal unity through the structure, indicating the complete tunneling. The imaginary part of the Poynting vector has its peaks at the ENG/DPS interfaces.

7. CONCLUSION

In this paper, we have studied the TE wave propagation in lossless trilayer stacks containing SNG materials. The following combinations have been considered: ENG/MNG/ENG, ENG/DPS/MNG, DPS/ENG/DPS, and ENG/DPS/ENG. Although the wave is evanescent into the SNG media, certain combinations of SNG layers or SNG and DPS layers lead to unusual features, such as the complete tunneling. The transfer-matrix formalism has been applied. Simple conditions for the complete tunneling were expressed analytically at normal incidence. The role of the material constants, layers thicknesses, and the incidence angle has been illustrated by numerical examples. In some cases, the comparison between the tunneling through the symmetrical trilayer stacks and that through the respective bilayer stacks has been provided. Besides the advantage of being predictable analytically [22], the complete tunneling through the symmetrical trilayer stacks is achieved in general on larger intervals of incidence angle variation in comparison with the respective bilayer stacks. We have analyzed also the field and the Poynting vector distributions inside and outside the trilayer stacks. In particular, we have shown that the complete tunneling is facilitated theoretically for the electrically thin stacks.

In our analysis the media have been assumed lossless. However, when dissipation is considered, the material constants are complex numbers, and the behavior of the electromagnetic tunneling through the trilayer stacks containing SNG materials can be drastically altered [7–9].

APPENDIX A. ELECTRIC- AND MAGNETIC-FIELD TANGENTIAL COMPONENTS INTO A TRILAYER STACK FOR THE TE CASE.

Consider a trilayer of material constants (ϵ_j, μ_j), with $j = 1, 2, 3$, and layers thicknesses $d_1/d_2/d_3$ placed in air at $z > 0$. Depending on the sign of material constants, the z component of the wave vector into an SNG or DPS layer is defined by (3). The tangential components E_y and $-H_x$ into the five regions can be written as follows,

$$\begin{aligned} z < 0, \quad E_y &= E_0 e^{-ixk_x}\left(e^{-izk_{z0}} + re^{izk_{z0}}\right) \\ -H_x &= \frac{k_{z0}}{\eta_0 k_0} E_0 e^{-ixk_x}\left(e^{-izk_{z0}} - re^{izk_{z0}}\right) \end{aligned} \tag{A1}$$

$$\begin{aligned} 0 < z < d_1, \quad E_y &= E_0 e^{-ixk_x}\left(f_{1+}e^{-izk_{z1}} + f_{1-}e^{izk_{z1}}\right) \\ -H_x &= \frac{k_{z1}}{\eta_0 k_0 \mu_1} E_0 e^{-ixk_x}\left(f_{1+}e^{-izk_{z1}} - f_{1-}e^{izk_{z1}}\right) \end{aligned} \tag{A2}$$

$$\begin{aligned} d_1 < z < d_1 + d_2, \\ E_y &= E_0 e^{-ixk_x}\left[f_{2+}e^{-i(z-d_1)k_{z2}} + f_{2-}e^{i(z-d_1)k_{z2}}\right] \\ -H_x &= \frac{k_{z2}}{\eta_0 k_0 \mu_2} E_0 e^{-ixk_x}\left[f_{2+}e^{-i(z-d_1)k_{z2}} - f_{2-}e^{i(z-d_1)k_{z2}}\right] \end{aligned} \tag{A3}$$

$$\begin{aligned} d_1 + d_2 < z < d_1 + d_2 + d_3, \\ E_y &= E_0 e^{-ixk_x}\left[f_{3+}e^{-i(z-d_1-d_2)k_{z3}} + f_{3-}e^{i(z-d_1-d_2)k_{z3}}\right] \\ -H_x &= \frac{k_{z3}}{\eta_0 k_0 \mu_3} E_0 e^{-ixk_x}\left[f_{3+}e^{-i(z-d_1-d_2)k_{z3}} - f_{3-}e^{i(z-d_1-d_2)k_{z3}}\right] \end{aligned} \tag{A4}$$

$$\begin{aligned} z > d_1 + d_2 + d_3, \quad E_y &= E_0 e^{-ixk_x} t e^{-i(z-d_1-d_2-d_3)k_{z0}} \\ -H_x &= \frac{k_{z0}}{\eta_0 k_0} E_0 e^{-ixk_x} t e^{-i(z-d_1-d_2-d_3)k_{z0}} \end{aligned} \tag{A5}$$

We use the following notations

$$A_\pm = \frac{1}{2}\left(1 \pm \frac{k_{z0}\mu_1}{k_{z1}}\right), \qquad B_\pm = \frac{1}{2}\left(1 \pm \frac{k_{z1}\mu_2}{k_{z2}\mu_1}\right), \tag{A6}$$

$$C_\pm = \frac{1}{2}\left(1 \pm \frac{k_{z2}\mu_3}{k_{z3}\mu_2}\right), \qquad D_\pm = \frac{k_{z3}}{k_{z0}\mu_3} \pm 1, \tag{A7}$$

$$\begin{aligned} P_\pm &= A_+ B_+ e^{\pm id_1 k_{z1}} + A_- B_- e^{\mp id_1 k_{z1}}, \\ Q_\pm &= A_- B_+ e^{\pm id_1 k_{z1}} + A_+ B_- e^{\mp id_1 k_{z1}}, \end{aligned} \tag{A8}$$

$$F = e^{-2id_2k_{z2}}\left(C_-D_+ - C_+D_-e^{-2id_3k_{z3}}\right),$$
$$G = C_+D_+ - C_-D_-e^{-2id_3k_{z3}}. \tag{A9}$$

Then, the amplitude reflection (r) and transmission (t) coefficients and the amplitude coefficients $f_{j\pm}$, with $j = 1, 2, 3$, are given by relations

$$r = -\frac{FP_- + GQ_+}{FQ_- + GP_+} \tag{A10}$$

$$\begin{aligned} f_{1\pm} &= A_\pm + rA_\mp, \\ f_{2\pm} &= f_{1+}B_\pm e^{-id_1k_{z1}} + f_{1-}B_\mp e^{id_1k_{z1}}, \\ f_{3\pm} &= f_{2+}C_\pm e^{-id_2k_{z2}} + f_{2-}C_\mp e^{id_2k_{z2}}, \end{aligned} \tag{A11}$$

$$t = f_{3+}e^{-id_3k_{z3}} + f_{3-}e^{id_3k_{z3}}. \tag{A12}$$

REFERENCES

1. Veselago, V. G., "The electrodynamics of substances with simultaneously negative values of permittivity and permeability," *Sov. Phys. Usp.*, Vol. 10, 509–514, 1968.
2. Smith, D. R., W. J. Padilla, D. C. Vier, S. C. Nemat-Nasser, and S. Schultz, "Composite medium with simultaneous negative permeability and permittivity," *Phys. Rev. Lett.*, Vol. 84, 4184–4187, 2000.
3. Pendry, J. B., "Negative refraction makes a perfect lens," *Phys. Rev. Lett.*, Vol. 85, 3966–3969, 2000.
4. Kong, J. A., "Electromagnetic wave interaction with stratified negative isotropic media," *Progress In Electromagnetics Research*, Vol. 35, 1–52, 2002.
5. Ran, L.-X., H.-F. Jiang Tao, H. Chen, X.-M. Zhang, K.-S. Cheng, T. M. Grzegorczyk, and J. A. Kong, "Experimental study on several left-handed metamaterials," *Progress In Electromagnetics Research*, Vol. 51, 249–279, 2005.
6. McCall, M. W., "What is negative refraction?," *Journal of Modern Optics*, Vol. 56, 1727–1740, 2009.
7. Alu, A. and N. Engheta, "Pairing an epsilon-negative slab with a mu-negative slab: Resonance, tunneling and transparency," *IEEE Trans. Antennas Propagation*, Vol. 51, 2558–2571, 2003.
8. Dong, L., G. Du, H. Jiang, H. Chen, and Y. Shi, "Transmission properties of lossy single-negative materials," *J. Opt. Soc. Am. B*, Vol. 26, 1091–1096, 2009.

9. Lin, W.-H., C.-J. Wu, and S.-J. Chang, "Angular dependence of wave reflection in a lossy single-negative bilayer," *Progress In Electromagnetics Research*, Vol. 107, 253–267, 2010.
10. Ding, Y., Y. Li, H. Jiang, and H. Chen, "Electromagnetic tunneling in nonconjugated epsilon-negative and mu-negative metamaterial pair," *PIERS Online*, Vol. 6, No. 2, 109–112, 2010.
11. Feng, T., Y. Li, H. Jiang, Y. Sun, L. He, H. Li, Y. Zhang, Y. Shi, and H. Chen, "Electromagnetic tunneling in a sandwich structure containing single negative media," *Phys. Rev. E*, Vol. 79, 026601, 2009.
12. Zhou, L., W. Wen, C. T. Chan, and P. Sheng, "Electromagnetic-wave tunneling through negative-permittivity media with high magnetic fields," *Phys. Rev. Lett.*, Vol. 94, 243905, 2005.
13. Tai, G.-C., C.-H.Chen, and Y.-W. Kiang, "Plasma-dielectric sandwich structure used as a tunable bandpass microwave filter," *IEEE Trans. Microwave Theory Tech.*, Vol. 32, 111–113, 1984.
14. Jiang, H., H. Chen, H. Li, Y. Zhang, J. Zi, and S. Zhu, "Properties of one-dimensional photonic crystals containing single-negative materials," *Phys. Rev. E*, Vol. 69, 066607, 2004.
15. Wang, L. G., H. Chen, and S. Y. Zhou, "Omnidirectional gap and defect mode of one-dimensional photonic crystals with single-negative materials," *Phys. Rev. B*, Vol. 70, 245102, 2004.
16. Yeh, D.-W. and C.-J. Wu, "Analysis of photonic band structure in a one-dimensional photonic crystal containing single-negative material," *Optics Express*, Vol. 17, 16666–16680, 2009.
17. Yeh, D.-W. and C.-J. Wu, "Thickness-dependent photonic bandgap in a one-dimensional single-negative photonic crystal," *J. Opt. Soc. Am. B*, Vol. 26, 1506–1510, 2009.
18. Rahimi, H., "Backward Tamm states in 1D single-negative metamaterial photonic crystals," *Progress In Electromagnetics Research Letters*, Vol. 13, 149–159, 2010.
19. Rahimi, H., A. Namdar, S. Roshan Entezar, and H. Tajalli, "Photonic transmission spectra in one-dimensional Fibonacci multilayer structures containing single-negative metamaterials," *Progress In Electromagnetics Research*, Vol. 102, 15–30, 2010.
20. Orfanidis, S. J., *Electromagnetic Waves and Antennas*, Chapter 6, Rutger University, 2008, www.ece.rutgers.edu/∼orfanidi/ewa.
21. Lakhtakia, A. and C. M. Krowne, "Restricted equivalence of paired epsilon-negative and mu-negative layers to a negative phase-velocity material (alias left-handed material)," *Optik*, Vol. 114, No. 7, 305–307, 2003.

22. Feng, S., "Graphical retrieval method for orthorhombic anisotropic materials," *Optics Express*, Vol. 18, 17009–17019, 2010.